The interaction between strain-rate and rotation in shear flow turbulence from inertial range to dissipative length scales

O. R. H. Buxton,[1,a)] S. Laizet,[1] and B. Ganapathisubramani[1,2]
[1]*Department of Aeronautics, Imperial College London, London SW7 2AZ, United Kingdom*
[2]*School of Engineering Sciences, University of Southampton, Southampton SO17 1BJ, United Kingdom*

(Received 4 February 2011; accepted 12 May 2011; published online 23 June 2011)

Direct numerical simulation data from the self similar region of a planar mixing layer is filtered at four different length scales, from the Taylor microscale to the dissipative scales, and is used to examine the scale dependence of the strain-rotation interaction in shear flow turbulence. The interaction is examined by exploring the alignment between the extensive strain-rate eigenvector and the vorticity vector. Results show that the mechanism for enstrophy amplification (propensity of which increases when the two vectors are parallel) is scale dependent with the probability of the two vectors being parallel higher for larger length scales. However, the mechanism for enstrophy attenuation, i.e., the probability of the two vectors being perpendicular to each other, appears to be scale independent. © *2011 American Institute of Physics*. [doi:10.1063/1.3599080]

The dynamics and evolution of the velocity gradient tensor, $D_{ij}=\partial u_i/\partial x_j$, have provoked great interest since the work of Vieillefosse.[1] The interaction between the strain-rate (S_{ij}) and rotation (Ω_{ij}) tensors, the symmetric and skew-symmetric parts of the velocity gradient tensor respectively, has been described as "intrinsic to the very nature of three dimensional turbulence."[2] It can be seen below that strain-rate and rotation both feature in the equations governing each others' dynamics.

$$\frac{1}{2}\frac{\mathrm{D}\omega_i^2}{\mathrm{D}t}=\omega_i S_{ij}\omega_j+\nu\omega_i\nabla^2\omega_i \tag{1}$$

$$\frac{1}{2}\frac{\mathrm{D}(S_{ij}S_{ij})}{\mathrm{D}t}=-S_{ij}S_{jk}S_{ki}-\frac{1}{4}\omega_i S_{ij}\omega_j-S_{ij}\frac{\partial^2 p}{\partial x_i\partial x_j}+\nu S_{ij}\nabla^2 S_{ij}. \tag{2}$$

The quantity $\omega_i S_{ij}\omega_j$, where $\omega_i=-\varepsilon_{ijk}\Omega_{jk}$ is the ith component of vorticity, is the rate of amplification of enstrophy and is an excellent metric for examining the interaction between strain and rotation.[3] This can be observed by rewriting it as[4]

$$\omega_i S_{ij}\omega_j=\omega^2 s_i(\hat{\mathbf{e}}_\mathbf{i}.\hat{\omega})^2, \tag{3}$$

where s_i are the eigenvalues of S_{ij} with corresponding eigenvectors $\boldsymbol{e_i}$, $\omega^2=\omega_\mathrm{i}\omega_\mathrm{i}$ and $\hat{\omega}=\omega/|\omega|$ is the vorticity unit vector. In an incompressible flow, the eigenvalues of S_{ij} can be ordered such that s_1 is always positive (extensive), s_3 is always negative (compressive), and s_2 is the intermediate eigenvalue which can be either (mildly) extensive or compressive and is bounded by the values of s_1 and s_3. The magnitude of the cosine of the alignment angles between the principle directions of the strain-rate tensor and the vorticity vector is thus of critical importance to determining the nature of enstrophy amplification.[5] These alignments have been studied extensively with the preponderance of the vorticity vector to be aligned in parallel with the intermediate strain-rate eigenvector first observed by Ashurst[6] and subsequently confirmed by several other studies.[7–9] In contrast, the vorticity vector has been shown to be preferentially aligned perpendicularly to the compressive strain-rate eigenvector. The alignment between the vorticity vector and the extensive strain-rate eigenvector has been shown to be arbitrary, leading to a "flat" *pdf*. Explanations for these alignments have been offered in other studies in the literature.[7,9] These alignment tendencies have also been found to be qualitatively similar in free shear flows[10,11] to homogeneous isotropic turbulence. The global tendency for the vorticity vector to be aligned in parallel with the intermediate strain-rate eigenvector and perpendicularly to the compressive strain-rate eigenvector is also evident in compressible turbulence;[12] however, there is a tendency for the extensive strain-rate eigenvector to be aligned in parallel with the vorticity vector although this is small in comparison with the other two alignment tendencies.

Insights into the strain–rotation interaction can also be gained by investigating two of the invariants of the velocity gradient tensor,[13] namely

$$Q=-\frac{1}{2}D_{ij}D_{ji}=\frac{1}{2}\left(\frac{1}{2}\omega_i^2-S_{ij}S_{ij}\right), \tag{4}$$

$$R=-\frac{1}{3}D_{ij}D_{jk}D_{ki}=-\frac{1}{3}S_{ij}S_{jk}S_{ki}-\frac{1}{4}\omega_i S_{ij}\omega_j. \tag{5}$$

Q can thus be physically interpreted as the local excess of rotation over strain-rate, and R can be interpreted as the local excess of strain amplification over enstrophy amplification. In addition, the condition of homogeneity in turbulence, first obtained by Townsend[14] and Betchov,[4] states the following:

$$\langle\omega_i^2\rangle=2\langle S_{ij}S_{ij}\rangle, \tag{6}$$

$$\langle -S_{ij}S_{jk}S_{ki}\rangle=\frac{3}{4}\langle\omega_i S_{ij}\omega_j\rangle. \tag{7}$$

Q and R can thus also be interpreted as local departures from homogeneity with regards to strain/rotation and strain/

[a)]Present address: Center for Aeromechanics Research, The University of Texas at Austin, Austin, Texas 78712-1085, USA.

rotation amplification rates, respectively. Four distinct sectors can be identified within the Q–R space, defined by the discriminant of the characteristic equation for the velocity gradient tensor, D, and R. When $D>0$, the characteristic equation for the velocity gradient tensor has one real and a complex conjugate pair of roots.[15] Regions for which $D>0$ are thus swirling regions, with the swirling strength defined by the magnitude of the imaginary part of the roots.[16] The fact that $\langle \omega_i S_{ij} \omega_j \rangle > 0$, that is to say, that enstrophy amplification is favoured over enstrophy attenuation, has been known since Taylor.[17] However, Buxton and Ganapathisubramani[18] showed that enstrophy attenuation ($\omega_i S_{ij} \omega_j < 0$) is strongly favoured in the sector for which $D>0$; $R>0$ (S1 in their terminology) of the Q–R space, whilst enstrophy amplification ($\omega_i S_{ij} \omega_j > 0$) is strongly favoured in the sector for which $D>0$; $R<0$ (S4) of their turbulent jet data. The mechanism responsible for this vortex is stretching. The vorticity vector was found to be aligned in parallel to the extensive strain-rate eigenvector ($\boldsymbol{e_1}$) in the enstrophy amplifying sector S4 and perpendicular to the extensive strain-rate eigenvector in the enstrophy attenuating sector S1. It was thus noted that despite the preference for the vorticity vector to be aligned to the intermediate strain-rate eigenvector, it was in fact the alignment between the vorticity vector and the extensive strain-rate eigenvector that was the most critical in determining the nature of enstrophy amplification. This preferential parallel alignment between $\boldsymbol{e_1}$ and $\boldsymbol{\omega}$ for enstrophy amplification and preferential perpendicular alignment for enstrophy attenuation was additionally observed for the whole flow, across all four sectors. Tsinober *et al.*[5] and Kholmyansky *et al.*[19] also noted that regions in which the vorticity vector is aligned with $\boldsymbol{e_1}$ play the most significant role in enstrophy amplification ($\omega_i S_{ij} \omega_j > 0$). The combination of these two different physical processes of preferential parallel alignment for $\omega_i S_{ij} \omega_j > 0$ and preferential perpendicular alignment for $\omega_i S_{ij} \omega_j < 0$ leads to the flat *pdf* for $\boldsymbol{e_1}$–$\boldsymbol{\omega}$ alignment that is often reported in the literature.

This interaction is inherently multi-scale in nature, and the physical process of vortex stretching via the interaction between strain and rotation is not necessarily universal at all length scales.[12] Therefore, the aim of this study is to examine the scale dependence of the alignment between $\boldsymbol{e_1}$ and $\boldsymbol{\omega}$ in shear flow turbulence and hence the mechanism for determining the nature of enstrophy amplification, by examining shear flow turbulence in the self similar region of a nominally two dimensional planar mixing layer.

The mixing layer is generated by means of a direct numerical simulation (DNS) using an in house code called "incompact3d" on a Cartesian grid, that is stretched in the cross stream direction, consisting of $2049 \times 513 \times 256$ nodes. The code is based on sixth order compact schemes for spatial discretization and a second order Adams-Bashforth scheme for time advancement. A Poisson equation for the pressure is solved in spectral space on a staggered grid. This code has been previously validated and further details of the numerical methods can be found in Laizet and Lamballais[20] and the boundary/initial conditions for the computation of a mixing layer found in Laizet *et al.*,[21] in which the thin trailing edge (TTE) case corresponds to the simulation in this study. A section of the computational domain, 750 η (301 nodes) in streamwise extent (where η is the Kolmogorov scale calculated from the original DNS data) from the centre of the mixing layer, just upstream of the end of the domain (which is 108 splitter plate widths), is isolated from four instantaneous snapshots. The cross stream extent of this section is 395η (159 nodes) which is similar to the vorticity thickness of the mixing layer where the mean shear is approximately uniform. This section is within the self similar region of the mixing layer and the Reynolds number based on the Taylor microscale (λ), calculated assuming local axisymmetry, is $Re_\lambda \approx 180$. The streamwise extent of the section is small in comparison to the development length of the mixing layer meaning that there is a negligible variation of the mean shear in the streamwise direction, and the mean shear in the cross stream direction is comparable to similar studies.[10,11] This domain is mean filtered onto regular Cartesian grids at four different resolutions 2.5η, 5η, 7.5η, and $25\eta \approx \lambda$. A magnitude of velocity gradient tensor $|D_{ij}|$ threshold is used to determine regions of the flow within the turbulent mixing layer and discount any potential flow.

Figure 1(a) shows the mean power spectral density for fluctuations in the streamwise direction of the isolated section of the computational domain in the streamwise, cross stream and spanwise directions (x_1, x_2, and x_3, respectively) as a function of wavenumber, where $k_i = 2\pi\Lambda_i$ is the wavenumber associated with the length scale in the direction of interest, Λ_i. The three filter widths that are above the Nyquist frequency that have been used to mean filter the data have

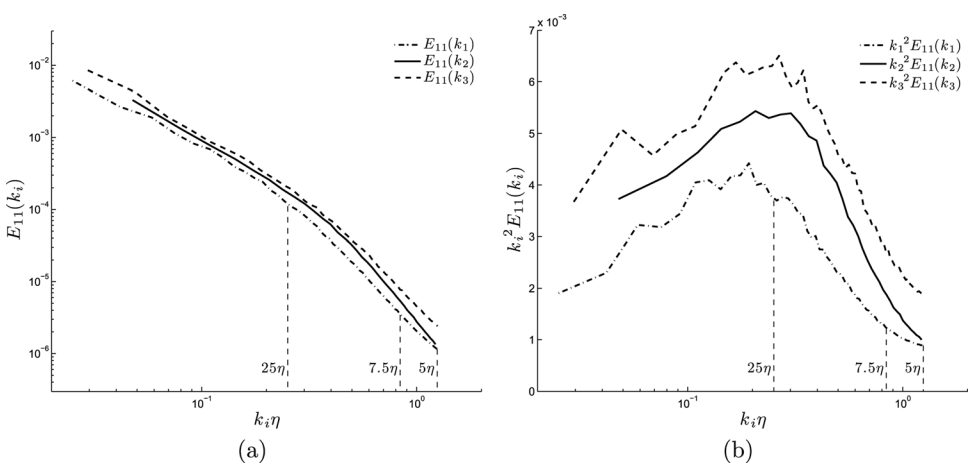

FIG. 1. (a) Mean power spectral density as a function of wavenumber ($E_{11}(k_i)$). (b) Mean dissipation spectrum as a function of wavenumber ($k_i^2 E_{11}(k_i)$). The three filter widths greater than the Nyquist frequency used in this study are illustrated on the figures.

been marked onto the figure. The two largest filter widths can be observed to lie at the extremes of the inertial range of scales, whereas the two smallest filter widths are within the dissipative range of scales. The smallest filter width, 2.5η, corresponds to the original streamwise (and spanwise) spacing of the grid upon which the DNS was computed and is not marked as no spectral information is available for the wavelength corresponding to this length scale. Mean filtering the data at these length scales can be thought of as discarding the contribution of all scales at wave numbers beyond that of the filter; hence, the filter width of 7.5η effectively discounts the contribution of the entire range of dissipative scales. This is illustrated in Fig. 1(b) which shows the dissipation spectrum, $k_i^2 E_{11}(k_i)$. Integrating this function between $k_1 = 0$ and $k_1\eta = 2\pi/7.5$ reveals that approximately 84% of the dissipation occurs at wavenumbers smaller than $2\pi/7.5\eta$ (hence some 16% occurs between $k_1\eta = 2\pi/7.5$ and $k_1\eta = 2\pi/5$). Approximately 34% of the total dissipation occurs at length scales greater than the largest filter width of $25\eta \approx \lambda$.

The effect of filter width upon the strain–rotation interaction is illustrated in Fig. 2, which displays contours of the joint probability density function ($pdf = 30$) between the second (Q) and third (R) invariants of the characteristic equation for the velocity gradient tensor, D_{ij}. In P–Q–R space, where $P = \nabla.\boldsymbol{u}$ is the first invariant of the characteristic equation of the velocity gradient tensor, the discriminant separating purely real from complex solutions can be given by[13]

$$27R^2 + (4P^3 - 18PQ)R + (4Q^3 - P^2Q^2) = 0. \qquad (8)$$

Thus in incompressible flow ($P = \nabla.\boldsymbol{u} = 0$) the discriminant, D, for the characteristic equation can be given by $D = Q^3 + 27/4R^2$. The dashed lines on the figure mark $D = 0$ and $R = 0$, which are used to split the two dimensional Q–R space into four separate sectors.

Figure 2 shows that as the filter width is increased from 2.5η to 7.5η there is an increase in the significance of the two swirling sectors (complex conjugate roots to the characteristic equation), S1 and S4. This is coupled to a decrease in the significance of the two strain dominated sectors for which the roots are purely real, S2 and S3. It can thus be concluded that larger length scales are dominated by swirling regions and smaller scales are strain dominated (dissipative). Equation 4 shows that Q is a measure of the local excess of rotation over strain and clearly this excess is greater at larger length scales.

The two sectors dominated by rotational motions, S1 and S4, are principally responsible for enstrophy attenuation and amplification, respectively. The primary mechanism for determining the sign of $\omega_i S_{ij} \omega_j$ and thus whether there is an attenuation or amplification of enstrophy is the alignment between $\boldsymbol{e_1}$ and $\boldsymbol{\omega}$.[18] Figure 3 shows probability density functions (*pdf*s) for the magnitude of the alignment cosine between $\boldsymbol{e_1}$ and $\boldsymbol{\omega}$ in the enstrophy amplifying ($\omega_i S_j \omega_j > 0$) sector S4 at the various filter widths. For comparison the dashed line and crosses show the global alignment *pdf*s, across all four sectors, for the data filtered at 2.5η and 7.5η, respectively. There is a peak at $|\widehat{\mathbf{e}_1}.\widehat{\omega}| = 1$ for the *pdf*s generated at all filter widths. Since sector S4 has complex roots to the characteristic equation for the velocity gradient tensor it is dominated by swirling. The peaks at $|\widehat{\mathbf{e}_1}.\widehat{\omega}| = 1$ thus support the finding that the mechanism for enstrophy amplification is parallel alignment between the vorticity vector and the extensive strain-rate eigenvector in rotationally dominated regions of the flow. There is, however, an increasing likelihood of parallel alignment between the two vectors at larger length scales. The *pdf* from the data mean filtered at 25η is admittedly noisy (due to the reduced quantity of data) but follows the same trend as the other three *pdf*s for a more marked peak at $|\widehat{\mathbf{e}_1}.\widehat{\omega}| = 1$ as the filter width is increased. This increased tendency for parallel alignment between $\boldsymbol{e_1}$ and $\boldsymbol{\omega}$ is at the expense of parallel alignment between the intermediate strain-rate eigenvector, $\boldsymbol{e_2}$ and $\boldsymbol{\omega}$. The literature, starting with Ashurst *et al.*,[6] extensively reports the dominant

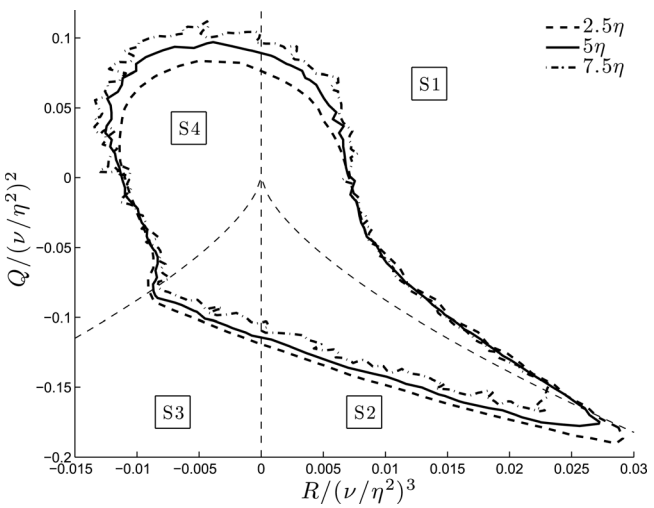

FIG. 2. Joint probability density function (*pdf*) between the second invariant (Q) and the third invariant (R) of the characteristic equation for the velocity gradient tensor. The dashed lines mark $R = 0$ and $D = 0$, where D is the discriminant of the characteristic equation.

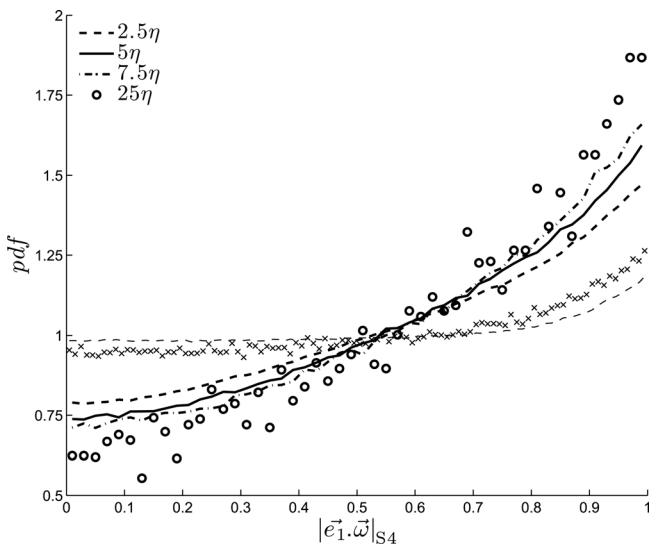

FIG. 3. Probability density function (*pdf*) for the magnitude of the alignment cosine between the extensive strain-rate eigenvector ($\boldsymbol{e_1}$) and the vorticity vector ($\boldsymbol{\omega}$) in sector S4 of the Q–R plot of Fig 2. The dashed line and the crosses are the global *pdf*s, across all four sectors, for the data filtered at 2.5 and 7.5η, respectively.

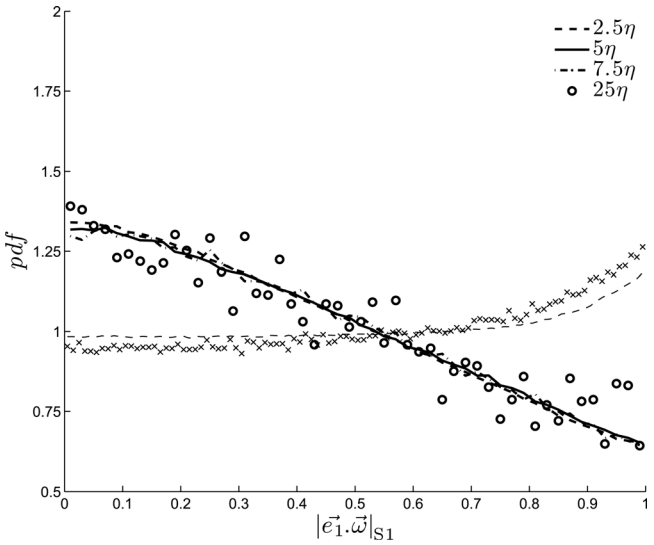

FIG. 4. *pdf* for the magnitude of the alignment cosine between $\boldsymbol{e_1}$ and $\boldsymbol{\omega}$ in sector S1 of the *Q–R* plot of Fig 2. The dashed line and the crosses are the global *pdf*s, across all four sectors, for the data filtered at 2.5 and 7.5η, respectively.

tendency for $\boldsymbol{e_2}$ and $\boldsymbol{\omega}$ to be aligned in parallel. It is observed, but not shown for brevity, that the tendency for $\boldsymbol{e_2}$ and $\boldsymbol{\omega}$ to be aligned in parallel decreases as the filter width is increased. For the two largest filter widths of 7.5η and 25η, which are at the two extremes of the inertial range of Fig. 1, parallel alignment between $\boldsymbol{e_1}$ and $\boldsymbol{\omega}$ is more probable than between $\boldsymbol{e_2}$ and $\boldsymbol{\omega}$. These findings suggest that enstrophy amplification is a process that takes place over a wide range of length scales, from large scales right down to the dissipative scales. The mechanism for enstrophy amplification is in fact more pronounced at inertial range scales than at the dissipative scales indicating that it is predominantly driven by larger scale structures.

Figure 4 shows *pdf*s of the magnitude of the alignment cosine between $\boldsymbol{e_1}$ and $\boldsymbol{\omega}$ in sector S1 at the various filter widths. The dashed line and crosses again show the global alignment *pdf*s, across all four sectors, for the data filtered at 2.5η and 7.5η, respectively, for comparison. The preferential perpendicular alignment between $\boldsymbol{e_1}$ and $\boldsymbol{\omega}$ is highlighted by the fact that all the *pdf*s show peaks at $|\widehat{\mathbf{e}_1}.\widehat{\omega}| = 0$. However, unlike for the enstrophy amplifying mechanism of parallel alignment between the two vectors, this enstrophy attenuating mechanism is insensitive to filter width. Again, the data mean filtered at 25η is noisy; more so than in Fig. 3 as there is less data as a consequence of the fact that $\langle \omega_i S_{ij} \omega_j \rangle > 0$.[17] However, all four *pdf*s follow the same qualitative and quantitative trend.

It has been shown in this letter that there is a tendency for a greater proportion of shear flow turbulence to be rotationally dominated, rather than strain dominated, at larger length scales. There is thus a greater contribution to the enstrophy attenuating and amplifying sectors, S1 and S4, respectively, in *Q–R* space. It has previously been shown that the alignment tendency between the extensive strain-rate eigenvector and the vorticity vector is a mechanism that determines whether enstrophy is amplified or attenuated. Figure 3 shows that the enstrophy amplifying mechanism is scale dependent and is driven by larger, inertial range scale structures that cascade down to the dissipative scale structures. By contrast, Fig. 4 suggests that there is a scale independence to the enstrophy attenuating mechanism (at least in the range examined in this study). It must be noted that these conclusions are drawn from a mixing layer, in which there is an approximately uniform mean shear. Whilst it is anticipated that the mean shear will have a quantitative effect on these findings it is not expected to affect the qualitative findings of the scale dependence of the enstrophy amplifying mechanism and the scale invariance of the enstrophy attenuating mechanism.

The authors would like to thank EPSRC for their support (through a Doctoral Training Grant for ORHB and for computational time on HECToR through the Resource Allocation Panel). O.R.H.B. also gratefully acknowledges financial support from the Royal Aeronautical Society.

[1]P. Vieillefosse, "Local interaction between vorticity and shear in a perfect incompressible fluid," J. Phys. **43**(6), 837 (1982).
[2]H. Tennekes and J. L. Lumley, *A First Course in Turbulence* (MIT, Cambridge, MA, 1972).
[3]A. Tsinober, M. Ortenberg, and L. Shtilman, "On depression of nonlinearity in turbulence," Phys. Fluids **11**(8), 2291 (1999).
[4]R. J. Betchov, "An inequality concerning the production of vorticity in isotropic turbulence," J. Fluid Mech. **1**, 497 (1956).
[5]A. Tsinober, L. Shtilman, and H. Vaisburd, "A study of properties of vortex stretching and enstophy generation in numerical and laboratory turbulence," Fluid Dyn. Res. **21**, 477 (1997).
[6]W. T. Ashurst, A. R. Kerstein, R. M. Kerr, and C. H. Gibson, "Alignment of vorticity and scalar gradient with strain rate in simulated Navier-Stokes turbulence," Phys. Fluids **30**,2343 (1987).
[7]J. Jiménez, "Kinematic alignment effects in turbulent flows," Phys. Fluids A **4**(4), 652 (1992).
[8]A. Tsinober, E. Kit, and T. Dracos, "Experimental investigation of the field of velocity gradients in turbulent flows," J. Fluid Mech. **242**, 169 (1992).
[9]P. E. Hamlington, J. Schumacher, and W. J. A. Dahm, "Direct assessment of vorticity alignment with local and nonlocal strain rates in turbulent flows," Phys. Fluids **20**(111703), 1 (2008).
[10]J. A. Mullin and W. J. A. Dahm, "Dual-plane stereo particle image velocimetry measurements of velocity gradient tensor fields in turbulent shear flow II.Experimental results," Phys. Fluids **18**(035102), 1 (2006).
[11]B. Ganapathisubramani, K. Lakshminarasimhan, and N. T. Clemens, "Investigation of three-dimensional structure of fine-scales in a turbulent jet by using cinematographic stereoscopic PIV," J. Fluid Mech. **598**, 141 (2008).
[12]D. H. Porter, P. R. Woodward, and A. Pouquet, "Inertial range structures in decaying compressible turbulent flows," Phys. Fluids **10**(1), 237 (1998).
[13]M. S. Chong, A. E. Perry, and B. J. Cantwell, "A general classification of three-dimensional flow fields," Phys. Fluids A **2**(5), 765 (1990).
[14]A. A. Townsend, "On the fine-scale structure of turbulence," Proc. R. Soc. Lond. A **208**(1095), 534 (1951).
[15]A. E. Perry and M. S. Chong, "Topology of flow patterns in vortex motions and turbulence," Appl. Sci. Res. **53**, 357 (1994).
[16]J. Zhou, R. J. Adrian, S. Balachandar, and T. M. Kendall, "Mechanisms for generating coherent packets of hairpin vortices in channel flow," J. Fluid Mech. **387**, 353 (1999).
[17]G. I. Taylor, "Production and dissipation of vorticity in a turbulent fluid," Proc. R. Soc. Lond. A **164**(916), 15 (1938).
[18]O. R. H. Buxton and B. Ganapathisubramani, "Amplification of enstrophy in the far field of an axisymmetric turbulent jet," J. Fluid Mech. **651**, 483 (2010).
[19]M. Kholmyansky, A. Tsinober, and S. Yorish, "Velocity derivatives in the atmospheric surface layer at $Re_\lambda = 10^4$," Phys. Fluids **13**(1), 311 (2001).
[20]S. Laizet and E. Lamballais, "High-order compact schemes for incompressible flows: A simple and efficient method with quasi-spectral accuracy," J. Comp. Phys. **228**(16), 5989 (2009).
[21]S. Laizet, S. Lardeau, and E. Lamballais, "Direct numerical simulation of a mixing layer downstream a thick splitter plate," Phys. Fluids **22**(015104), 1 (2010).